IOSR Journal of Mechanical and Civil Engineering (IOSR-JMCE)
e-ISSN: 2278-1684, p-ISSN: 2320-334X, Volume 23, Issue 1 Ser. 1 (Jan - Feb 2026), PP 01-14
www.iosrjournals.org

Assessment Of Axial Stiffness Reduction Factors For Concrete T-Beams Under Thermal Loading

Osama Mantawy[1*], Hisham A. El-Arabaty[2], Mohamed A. Abdelwahab[3], Akram M. Abdelmaksoud[4]

(Assistant Lecturer Of Structural Engineering, Ain-Shams University, Egypt)
(Professor Of Structural Engineering, Ain-Shams University, Egypt)
(Assistant Professor Of Structural Engineering, Ain-Shams University, Egypt)
(Assistant Professor Of Structural Engineering, Ain-Shams University, Egypt)

Abstract:
Thermal analysis of reinforced concrete structures poses an important challenge in the analysis and design of buildings since the high axial stiffness of slabs and beams results in large lateral forces on the supporting columns and, consequently, high values of straining actions. In this research, an analytical algorithm is developed to assess beams and slabs axial stiffness, considering the effect of cracks caused by both vertical loads and temperature changes. The reason for this study is to determine the effect of pre-existing cracks resulted by bending moments of vertical loads on the beams' axial stiffness. A software package is developed to compute T-beams effective axial stiffness based on the degree of section cracking. Two methods are presented here to study T-beam axial stiffness under different points of application of the axial force. Different values of compression and tension forces on T-beam were studied to capture the effect of axial forces values on T-beam axial stiffness. A parametric study was performed to examine the effect of different parameters, such as T-beam reinforcement ratio and T-beam concrete dimensions on the axial stiffness reduction factors. These factors shall be used in thermal analysis of T-beams in finite element modeling of Reinforced Concrete buildings.

Key Words: *Axial Stiffness, Beams, Reduction Factors, Slabs, Thermal Analysis*

Date of Submission: 23-12-2025 Date of Acceptance: 03-01-2026

I. Introduction

Reinforced concrete structures are exposed to thermal loading, such as ambient conditions, temperature change, and exposure to fire. The thermal analysis of reinforced concrete structures is an integral part of the overall structural analysis, and it poses a unique concern in structural modeling. Furthermore, the thermal effect is more pronounced in the case of buildings with a large length in one or more directions and that have no expansion joints. Temperature variation produces axial forces on slabs and beams, which result in horizontal deformations, causing shear forces and bending moments on supporting columns, especially on the floors with their columns attached to the foundation due to the restraint imposed by footings. External columns experience greater horizontal displacements compared to interior columns since deformations increase far from slab center, which results in higher shear forces and bending moments. Modeling building horizontal elements such as slabs and beams with their gross area results in high axial stiffness of these elements. Applying changes in temperature on these elements leads to large horizontal forces which are transferred to supporting columns resulting in high straining actions and consequently a less economical design. Hence, reducing the axial stiffness of both floor beams and slabs results in more realistic values for straining actions on columns since beams and slabs are cracked under the effect of pre-existing vertical loads. Various codes of practice have specified certain reduction factors for use in the thermal analysis of structures[1-3]. Moreover, the use of a fixed reduction factor for all temperature cases in the analysis may not be appropriate as this reduction factor depends on the degree of cracking in elements. Thus, the accurate determination of slabs and beams axial stiffness is important to get more realistic values of straining actions on columns.

Another point to consider is that the beam and slab systems' analysis under thermal loading is affected by the resulting axial force location. In other words, the axial force can be considered acting at the centroid of the T-section formed by the beam itself and the effective width of slab contributing in beam stiffness when columns are directly connected to beams. On the other hand, in cases where columns are connected to slabs directly at some locations, the axial force acts at or near the slab center when the axial forces are transferred to the beam from the slabs.

This study concentrates on the accurate analysis of beams sections under bending moments caused by vertical loads as well as tension and compression forces to determine beams' axial stiffness under thermal loads. The aim of this study is to investigate the effect of concrete cracking on the axial stiffness of slabs and beams in order to make an assessment of suitable reduction factors for beams axial stiffness. A software package was prepared for the calculation of reduction factors for beams axial stiffness and this shall be presented in this research.

An in-depth study is performed to include all of the above cases, with the objective of determining the relevant values for stiffness reduction factors to be applied in the analysis to produce realistic results representing the actual thermal effect on the beams and slabs in both cases of expansion and contraction.

II. Literature Review

Several studies have been performed regarding the concrete cracking effect on the axial stiffness of slabs and beams either considering material nonlinearity or analyzing behaviour within the working load limits. Some of these studies are listed below as follows:

Salah E. El-Metwally 2019 [8,9] studied the effect of temperature variation and shrinkage on concrete flat plate systems and raft foundations. The study showed that temperature variation had a more significant effect on flat plate slabs than on rafts. The stresses in steel reinforcement were noticeably affected in rafts and significantly affected in slabs by temperature variations.

Mohamed Abdul Rahim 2018 [5,6] developed a software package for the assessment of the cracking effect on beam axial stiffness. The developed algorithm was based on iteratively running the ETABS program repeatedly, then using the results of axial force in the beams to determine the appropriate reduction factor for the beams' axial stiffness using the developed software. The parametric study results showed that the most important factor affecting the axial stiffness reduction factor was the amount of steel reinforcement in the beam section. It was also recommended not to use a single fixed value for the stiffness reduction factors for all cases of temperature in order to determine these factors accurately, which can lead to a reduction in the resulting straining actions in the supporting columns.

Heba A. Goda 2022 [4]. developed a software package for the assessment of the cracking effect on flat slab axial stiffness. The software was based on drawing the relationship between the cracked stiffness and the acting axial force at a specific bending moment value, then using the ETABS model to obtain the resulting axial force in the slab, which was then used in the developed software to determine the slab stiffness reduction factors. The parametric study showed that slabs with large thickness produced slightly smaller values for reduction factors than slabs with small thickness. The results also showed that an increase in beam tension steel significantly increased the slabs' cracked stiffness, resulting in higher reduction factors.

III. Development Of The Analytical Algorithm

The case of a T-section composed of a beam, and slab, under the effect of both bending moments and axial forces, is analyzed here at working loads level. The working load level was selected as it is commonly expected that the floor is subjected to temperature loads, while the vertical loads acting on it, are still within the working load level. While severe temperature-induced expansion and contraction of the floor slabs and beams might produce ultimate level stresses, and probable failure in columns, this can still occur while the beams and slabs are still within the working level stresses [5,6].

The strain diagram produced by a combination of axial forces and bending moments (N&M) acting on the T-beam section is illustrated in the following subsections, together with the relevant relations between these strain values, and the acting (N&M). Two cases are studied here, one is for the +ve moment case, and the other is for the -ve moment case. Where +ve moment represents the case where the tension side acts at the bottom of the section and -ve moment represents the case where the tension side acts at the top of the section.

Case (1) Axial forces & +VE Moments acting on section

The strain diagram caused by a combination of axial force and +ve bending moment acting on the beam section is shown in Figures 1a &1b. Figure. 1a. illustrates the case where the neutral axis location is in the beam, while Figure. 1b. illustrates the case where the neutral axis location is in the slab.

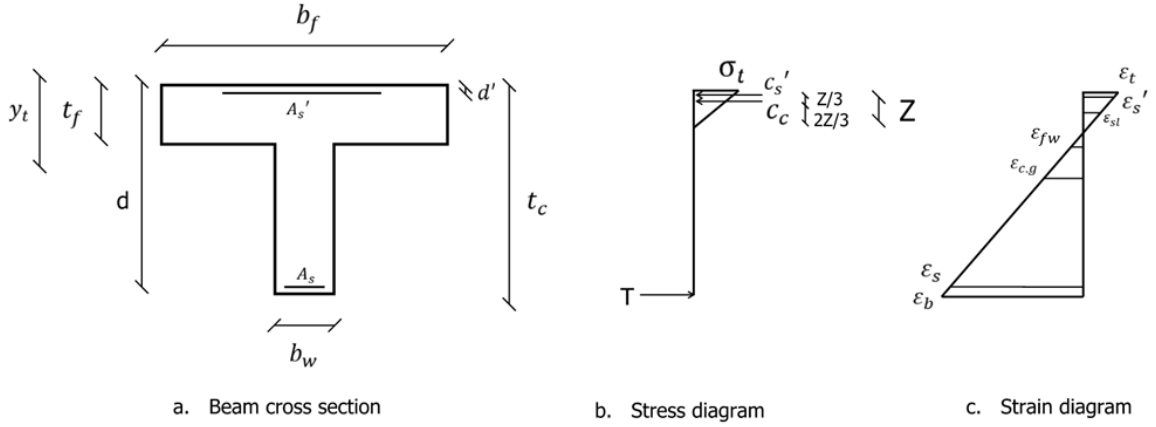

a. Case (A) z < t_f

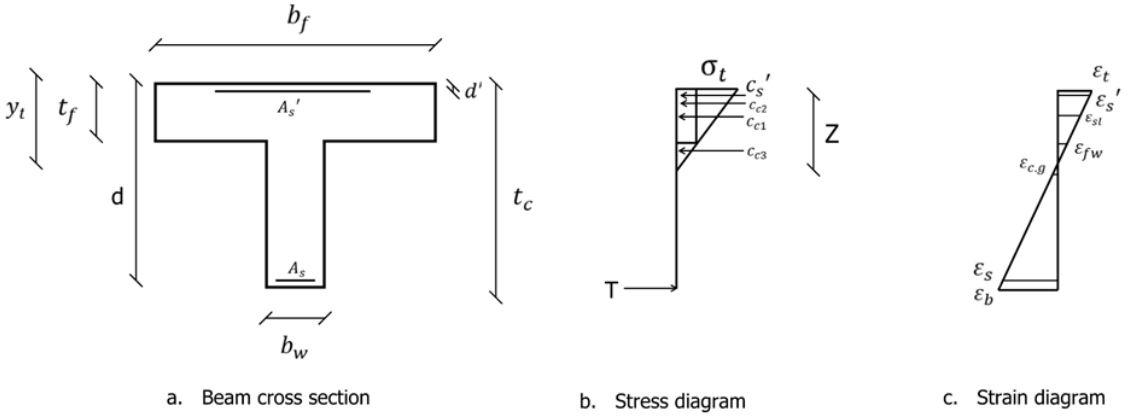

b. Case (B) z > t_f

Figure 1. Stress and strain diagrams for + ve moment case

Assuming the strains at the bottom and top of the beam cross section as (ε_b & ε_t) respectively, the other strain values indicated in the figure can be calculated relative to these values as follows:

$\varepsilon_s = (\varepsilon_t\ (t_c - d) + \varepsilon_b\ (\text{d})) / t_c$ (1)

$\varepsilon_s' = ((\varepsilon_t\ (t_c - d') + \varepsilon_b\ (\text{d}')) / t_c$ (2)

$\varepsilon_{c.g} = ((\varepsilon_t\ (t_c - y_t) + \varepsilon_b\ (y_t)) / t_c$ (3)

$\varepsilon_{fw} = ((\varepsilon_t\ (t_c - t_f) + \varepsilon_b\ (t_f)) / t_c$ (4)

$\varepsilon_{sl} = ((\varepsilon_t\ (t_c - t_f/2) + \varepsilon_b\ (t_f/2)) / t_c$ (5)

Also the stresses in concrete at the top of the beam section and at the intersection between flange and web can be derived as follows:

$\sigma_t = E_c * \varepsilon_t$ (6)

$\sigma_{fw} = E_c * \varepsilon_{fw}$ (7)

Where E_c is the concrete Young's modulus.

The neutral axis location relative to the top of the beam can be determined as follows:

$Z = (\varepsilon_t / (\varepsilon_t + \varepsilon_b))\ t_c$ (8)

The stresses and forces in steel reinforcement can be calculated as follows :

$T = A_s * E_s * \varepsilon_s$ (9)

$C_s' = A_s' * E_s * \varepsilon_s'$ (10)

Where E_s is the steel Young's modulus, T is the force in tensile steel reinforcement and C_s' is the force in compressive steel reinforcement.

For a specific beam section with fixed dimensions and fixed reinforcement values, since the strain variation is linear, multiplication of the strain diagram by any factor will result in all the strains being multiplied by the same factor. The normal force (N) and bending moment (M) values will increase by the same factor, and the resulting ratio of (M/N) will remain constant. This ratio does not depend on the specific values of the bottom and top beam strains ($\varepsilon_b, \varepsilon_t$) but depends only on the ratio between them. This concept will be utilized in the development of the flowchart and software used to determine the values of stiffness reduction factors in this study.

The corresponding forces of the concrete and the corresponding values of bending moment (M) and normal force (N) can be determined as follows:

Case (A) $z < t_f$

$c_c = (\sigma_t * Z) / 2 * b_f$ (11)

$N = c_c + c_s' - T$ (12)

$M = (c_c * (y_t - Z/3) + c_s' * (y_t - d') + T * (d - y_t))$ (13)

Case (B) $z > t_f$

$c_{c1} = (\sigma_{fw} * b_f * t_f)$ (14)

$c_{c2} = ((\sigma_t - \sigma_{fw}) / 2) * b_f * t_f$ (15)

$c_{c3} = (\sigma_{fw} * (Z - t_f) / 2) * b_w$ (16)

$c_c = c_{c1} + c_{c2} + c_{c3}$ (17)

$N = c_c + c_s' - T$ (18)

$M = (c_{c1} * (y_t - t_f/2) + c_{c2} * (y_t - t_f/3) + c_{c3} * (y_t - t_f - ((Z - t_f)/3)) + c_s' * (y_t - d') + T * (d - y_t)$ (19)

Where c_c is the compression force in concrete.

The strain diagram caused by a combination of axial force and -ve bending moment acting on the beam section is shown in Figures 2 a & 2b. Figure. 2a illustrates the case where the neutral axis location is in the beam, while Figure. 2b illustrates the case where the neutral axis is in the slab.

Case (2): Axial forces & -ve moments acting on section

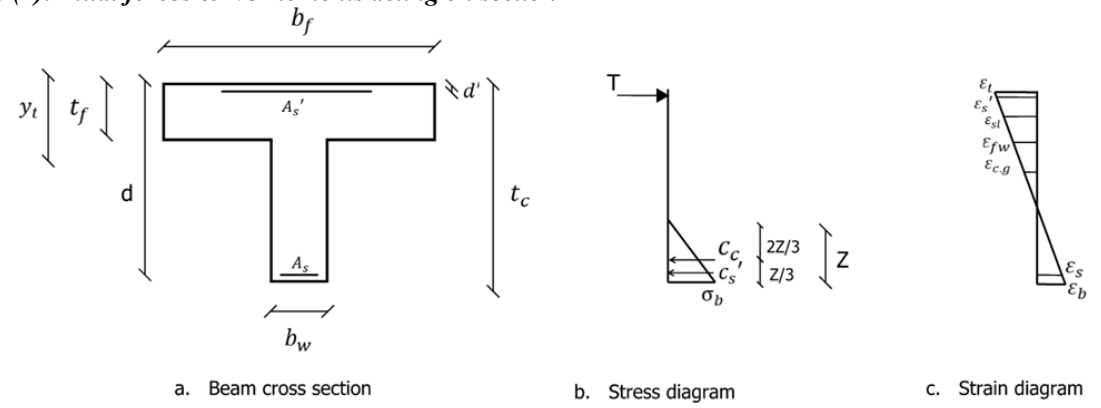

a. Beam cross section b. Stress diagram c. Strain diagram

a. Case (A) **a**. $z < (t_c - t_f)$

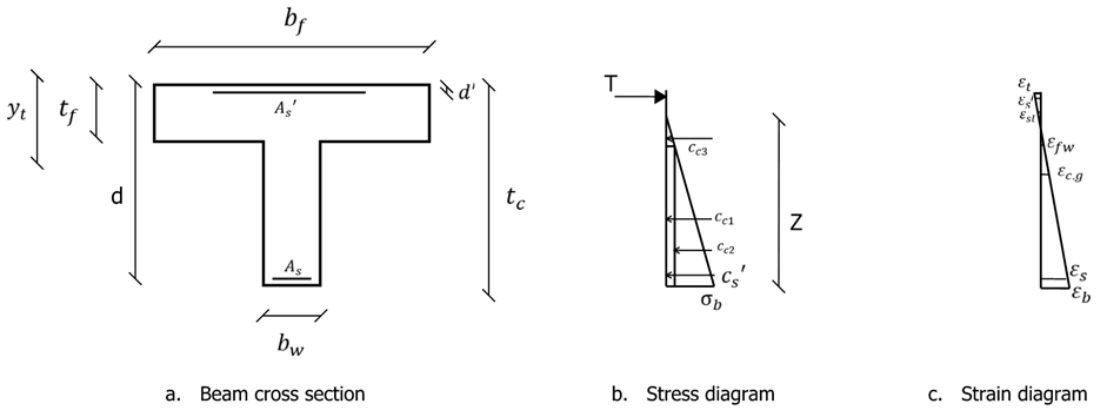

a. Beam cross section b. Stress diagram c. Strain diagram

b. Case (B) $z > (t_c - t_f)$

Figure 2. Stress and strain diagrams for -ve moment case

The same equations for the strain values and the stresses at the intersection between the flange and web can be used in the case of a negative moment acting on the beam section.

The stresses in concrete at the bottom of the beam section can be derived as follows:

$\sigma_b = E_c * \varepsilon_b$ (20)

Where E_c is the concrete Young's modulus.

The neutral axis location relative to the top of the beam can be determined as follows:

$Z = (\varepsilon_b / (\varepsilon_t + \varepsilon_b))\, t_c$ (21)

The stresses and forces in steel reinforcement can be calculated as follows :

$c_s' = A_s * E_s * \varepsilon_s$ (22)

$T = A_s' * E_s * \varepsilon_s'$ (23)

The corresponding forces of the concrete and the corresponding values of bending moment and normal force can be determined as follows:

Case (A) $z < t_w$

$c_c = (\sigma_b * Z) / 2 * b_w$ (24)

$N = c_c + c_s' - T$ (25)

$M = (c_c * (t_c - y_t - Z/3) + T * (y_t - d') + c_s' * (d - y_t))$ (26)

Case (B) $z > t_w$

$c_{c1} = (\sigma_{fw} * b_w * t_w)$ (27)

$c_{c2} = ((\sigma_b - \sigma_{fw}) / 2) * b_w * t_w$ (28)

$c_{c3} = (\sigma_{fw} * (Z - t_w) / 2) * b_f$ (29)

$c_c = c_{c1} + c_{c2} + c_{c3}$ (30)

$N = c_c + c_s' - T$ (31)

$M = (c_{c1} * (t_c - y_t - t_w/2) + c_{c2} * (t_c - y_t - t_w/3) + c_{c3} * ((t_w - (t_c - y_t)) + ((Z - t_w)/3)) + T * (y_t - d') + c_s' * (d - y_t))$ (32)

Analytical Methodology for axial stiffness computation:

By varying the $(\varepsilon_b/\varepsilon_t)$ ratio, the corresponding (M/N) ratio can be calculated for a specific section. The algorithm used is based on calculating (M/N) ratio for a wide range of $(\varepsilon_b/\varepsilon_t)$ ratios, at specific steps, and saving the resulting values in matrix form, and subsequently using them as a base for calculations of the T-section beam axial stiffness values.

At a specific value of the acting bending moment (generally caused by vertical loads), the strain diagram corresponding to this level of moment can be determined form the above-mentioned matrix. The addition of an axial force to this moment value results in a shift in the strain diagram. The new strain diagram corresponding to the (N&M) values can be calculated. From the two diagrams, change in strain (and consequently displacement) at the section centroid is computed, to be used in calculation of the axial stiffness value. This axial stiffness corresponds to the realistic deformations due to the axial force acting on a cracked seciton, already under the effect of acting vertical load moments. This represents the actual case while beam section is cracked under bending moments due to applied vertical loads, and the level of cracking affects affects the induced strain and displacement resulted by normal forces formed from thermal effects. A graph can subsequently be plotted between the centroid strain $\varepsilon_{c.g}$ (or deformation Δ), and the corresponding axial load (N) for a specific value of bending moment (M). Figure. 3. illustrates the typical variation of acting axial force and deformation at seciton C.G for a cracked section. The section cracked stiffness can be caluclated using the secant stiffness, as shown.

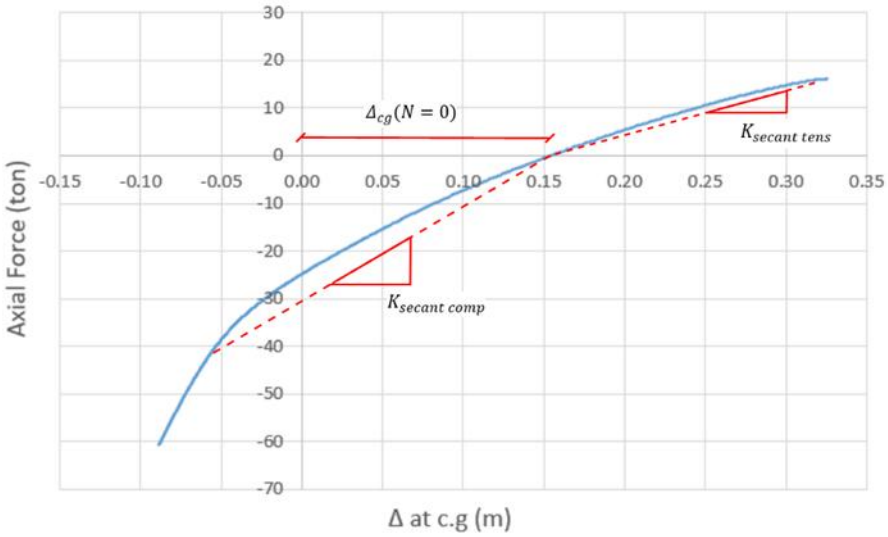

Figure 3. Axial force-Displacement relationship

The secant stiffness (Ksecant), is computed for both compression and tension cases, through computation of the slope of the secant starting from the point of zero force, to the required point, whether it represents compression or tension forces, acting on the section. As explained previously, several cases occur in actual

beam/slab floors, which cause differences in the point of application of the axial forces resulting from expansion/contraction of floors. Therefore, two different approaches were proposed here, and used to determine the axial stiffness reduction factors of the concrete T-beams. A summary of the two used approaches are presnted in Table.1.

Table 1. Force and strain locations for the described two approaches in +ve &-ve moment cases.

Method No.	Point of Applied Force	Point of measured Strain	Moment direction
Approach 1A	Section centroid	Section centroid	Positive
Approach 2A	Center of slab	Center of slab	Positive
Approach 1B	Section centroid	Section centroid	Negative
Approach 2B	Center of slab	Center of slab	Negative

Calculating reduction factors based on the two approaches is described as follows:

Approach 1A:Force acting at section CG,and deformation measured at section CG under the effect of positive moment and axial force

As shown in Figure.4, this method depends on assuming the normal Force acting at C.G and calculating the corresponding strains. Then, displacements values can be extracted from resulted strains to be used in stiffness calculations. Stiffness reduction factor can be calculated as follows:

$K_{secant} = P_{axial} / (\Delta_{cg} - \Delta_{cg}(N = 0))$ (33)

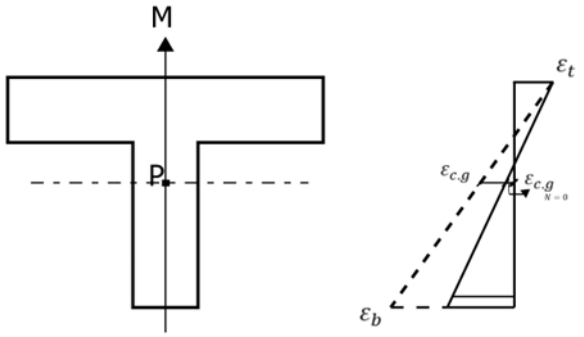

Figure 4. Force acting at C.G & Strain calculation at C.G for +VE moment case

While the realistic axial stiffness based on the cracked beam sections can be represented by K_{Secant} which can be K_{Comp} in case of copressive forces and K_{Tens} in case of tensile forces. By dividing this value by gross axial stiffness of the beam (EA/L), reduction factors can be extracted representing the effect of the level of cracking on beam axial stiffness. For a beam length of 1 meter, $\varepsilon_{c.g} = \Delta_{cg}$ and the reduction factors can be calculated as follows :

$RF_{comp} = K_{Comp} / (EA/L)$ (34)

$RF_{tens} = K_{Tens} / (EA/L)$ (35)

Approach 2A: Force acting at section slab center, and deformation measured at section slab center under positive moment and axial force

This method depends on assuming the normal force acting at the center of slab and calculating the corresponding strains. The eccentricity (e) of the acting force can be defined as the distance between the acting force and the centroid of the beam cross section as follows:

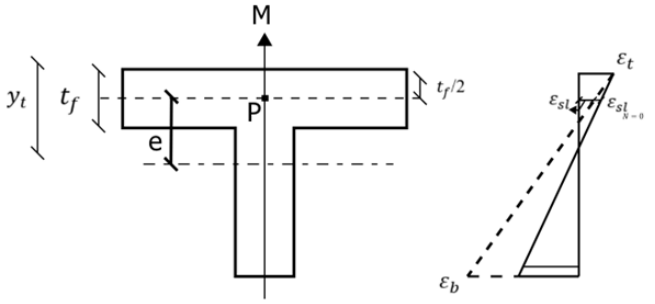

Figure 5. Force acting at S.C & Strain calculation at S.C for +VE moment case

This method depends on assuming the normal force acting at the center of slab and calculating the corresponding strains. The eccentricity (e) of the acting force can be defined as the distance between the acting force and the centroid of the beam cross section as follows:

$e = y_t - (t_f/2)$ (36)

The stress diagram shown in Figure 5 is considered here as a result of both the bending moment due to the vertical loads and the normal force in addition to the moment resulting from it due to the eccentricty. The moment due to vertical loads alone can be calculated as follows:

$M_{VL} = M_{tot} - P\ x\ e$ (37)

By scaling these moment values to the external moment values caused by vertical loads we can get a relationship between the normal force and strains at slab center as follows:

Scale factor (F) $= M_{ex} / M_{VL}$ (38)

Where M_{ex} is the moment due to the vertical loads acting on the beam.The scaled forces and strains can be calculated as follows :

$P_{sc} = P\ x\ F$ (39)

$\varepsilon_{sc} = \varepsilon_{sl} x\ F$ (40)

Where ε_{sc} is the scaled strain at slab center, and the beam stiffness can be calculated as follows:

$K_{secant} = P_{sc} / (\Delta_{sc} - \Delta_{sc}(N = 0))$ (41)

Approach 1B: Force acting at section CG, and deformation measured at section CG under the effect of negative moment and axial force

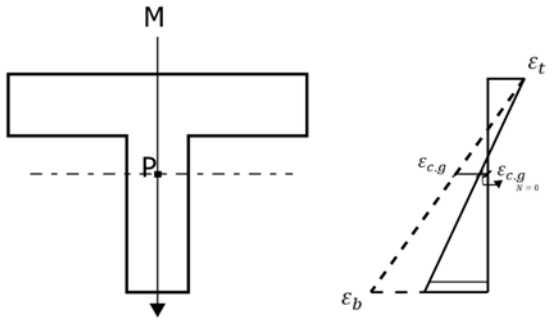

Figure 6. Force acting at C.G & Strain calculation at C.G for -VE moment case

As shown in Figure.6, this method depends on assuming the normal Force acting at C.G and calculating the corresponding strains at C.G. Stiffness reduction factor can be calculated as follows :

$K_{secant} = P_{axial} / (\Delta_{cg} - \Delta_{cg}(N = 0))$ (42)

$RF = K_{secant} / (EA/L)$ (43)

Approach 2B: Force acting at slab center , and deformation measured at slab section under the effect of negative moment and axial force

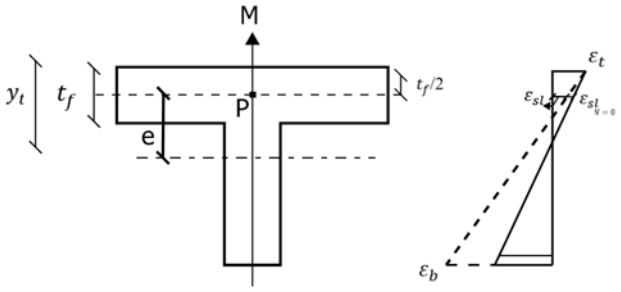

Figure 7. Force acting at S.C & Strain calculation at S.C for -VE moment case

As shown in Figure.7, This method is based on assuming the force acting at the center of slab and calculating the Stiffness modifier based on the strains at the center of slab. The eccentricity and scaling procedure can be calculated as described below:

$M_{VL} = M_{tot} + P\ x\ e$ (44)

Scale factor (F) $= M_{ex} / M_{VL}$ (45)

$P_{sc} = P\ x\ F$ (46)

$\varepsilon_{sc} = \varepsilon_{sl} x\ F$ (47)

And the secant stiffness can be calculated as follows :

$$K_{secant} = P_{sc} / (\Delta_{sc} - \Delta_{sc}(N = 0)) \quad (48)$$

IV. Analysis Results & Discussion

Results for the two previous cases (+ve & -ve moment) using the two approaches mentioned before are plotted against each other in the next figures against a single fixed value for the bending moment caused by the vertical loads. Figure 8a. shows the relationship between the axial forces acting on the beam and the corresponding stiffness reduction factors for the +ve moment case using approaches 1A & 2A. Figure 8b. shows the relationship between the acting axial forces and the corresponding stiffness reduction factors for the -ve moment case using approaches 1B&2B.

As shown in Figure. 8a., for the compression force case which represents the thermal expansion case, the beam axial stiffness increases significantly with the increase of the compression force. This can be illustrated by the fact that when the compression force acts on the beam which is already cracked due to the vertical loads, the compression force causes the closing of these cracks, which increases beam axial stiffness. For a range of compression forces (around 10 to 20 t), the reduction factor is around 0.22 in approach 1A, and it is increased to around 0.4 in case of approach 2A.

For the tension force case, which represents the thermal contraction case, the beam axial stiffness decreases, as when the tension force acts on the beam section, it causes an increase in cracks which were previously caused by vertical loads. This decreases the beam axial stiffness. For a range of tension forces (around 10 to 15t) , the reduction factor is decreased to less than 0.2 in case of approach 1A and around 0.25 in approach 2A.

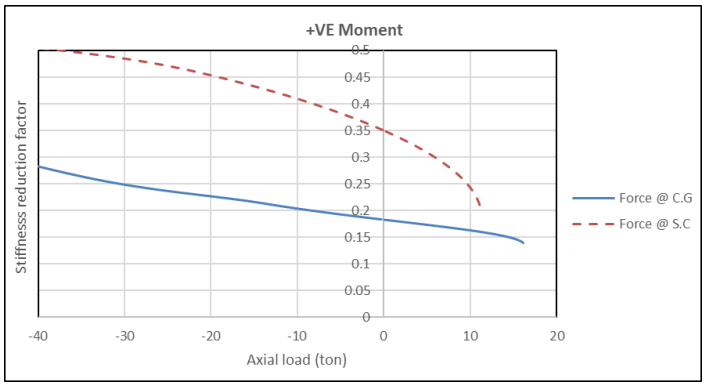

a. +VE moment case

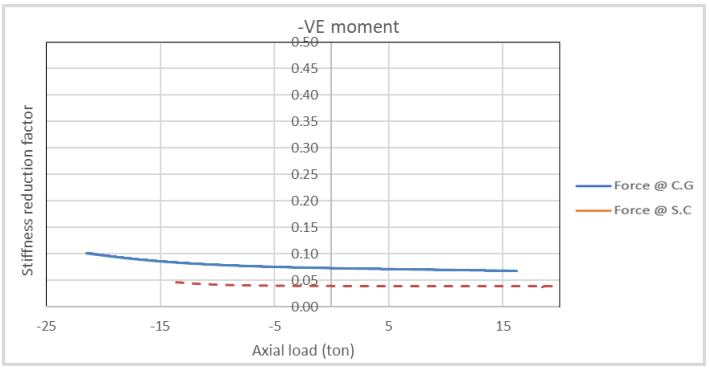

b. -VE moment case

Figure 8.: Variation of stiffness reduction factor with axial load for the two described methods.

It is noted in figure.8a, that for +ve moment cases, that in the case where the stiffness reduction factors (SRFs) are computed based on force and resulting displacement at the slab center, the SRFs are higher than the case where they are computed based on force and displacement acting at beam section centroid. This indicates that the SRFs (+ve M case) for the beam-slab T-section, are significantly higher, when thermal loads are transmitted between laterally deformed columns and slabs, and not to the beams. Fig. 8b shows a total reversal in case of –ve Moment acting at the section, where the SRFs are higher in the case where SRFs are computed based on force and displacement acting at beam section centroid.

The above phenomenon is very important to consider, when developing an understanding of the expected stiffness reduction, caused by section cracking in the T-section beams transferring thermal loads from one side of

the building to the other, as part of the overall slab structure. It can be explained by the additional moments developed when the axial forces are transferred in a higher percentage through the slab, as its eccentricity from the overall T-section C.G produces these moments.

As shown in Figure.8a & 8b, stiffness reduction factors are higher in case of positive moment acting on the beam section, than in the case of negative moment. This applies to both cases of tension and compression axial forces produced by the thermal effect. This is caused by the pre-existing cracking in the top flange in the case of -ve moment due to tensile stresses resulting from the bending moment caused by vertical loads. This phenomenon is highly pronounced as illustrated in Figure 8b since the stiffness reduction factors are very low (reaching around 8%) in the case of negative moment acting at the section. Furthermore, this behaviour was captured for both cases of axial compression and tension forces acting at the beam centroid. This can be explained by the fact that in the -ve moment case, the flange, which contributes highly to the axial stiffness due to its relative area compared to the whole section area, is in tension which decreases the reduction factors. On the contrary, the flange in the +ve moment case is compressed without cracking, which increases the axial stiffness of the whole section resulting in higher reduction factors. Figure 9a&9b show the strain distribution along the beam section in the +ve moment case for both compression and tension forces. The strain diagrams through the section height shown in figures 9a &9b illustrate the behaviour causes these results for SRFs. In the case of +ve moment and a compression force, and taking the strain diagram of the zero normal force case as a reference, which shows the strain under vertical loads moment only, the strain diagram of N.F. acting at c.g is shifted to the right and rotated anti-clockwise. The difference between strain diagrams of N.F. equals zero and N.F. acting at C.G is the denominator of the cracked axial stiffness. In the case of N.F acting at S.C, the strain diagram is rotated clockwise in an opposite direction compared to the N.F acting at C.G, which decreases the difference between strain diagrams of N.F equals zero and N.F acting at S.C. Since this difference is the denominator of the cracked axial stiffness formula. This explains the increase in cracked axial stiffness in the case of N.F acting at S.C compared to the N.F acting at C.G case. A similar behaviour is noted in Figure 9b for the tension force case, as in case of N.F acting at S.C, the strain diagram is rotated anticlockwise in an opposite direction compared to the N.F acting at C.G which is rotated colckwise. This behaviour decreases the denominator of the cracked axial stiffness and also increases the cracked axial stiffness.

Figure 10a&10b show the strain distribution along the beam section in the -ve moment case for both compression and tension forces.

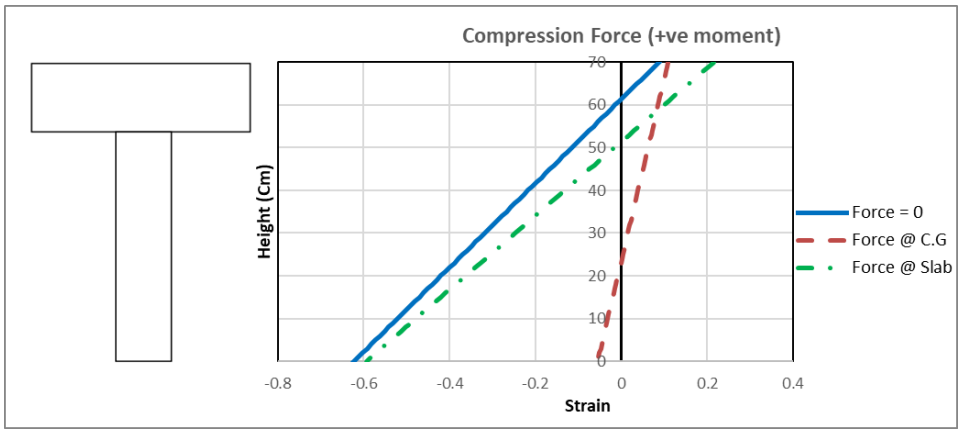

a. Compression force

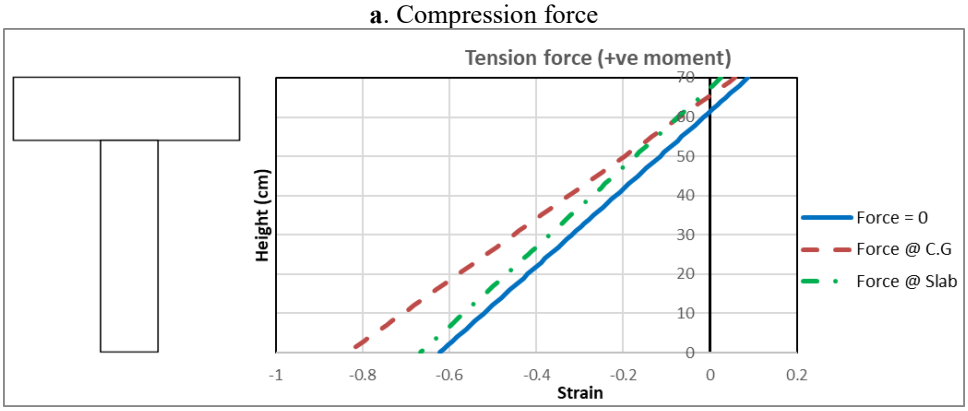

b. Tension force

Figure 9. : Strain distribution along T-Beam depth for +ve moment case using Method 1A&2A

Strain diagrams through the section height shown in figures 10a &10b illustrate the behaviour that causes these results for SRFs in the -ve moment case. In the case of -ve moment and a compression force, and taking the strain diagram of the zero normal force case as a reference, the strain diagram of N.F acting at c.g is shifted to the right and rotated clockwise. In the case of N.F acting at S.C, the strain diagram is rotated clockwise, in the same direction compared to the N.F acting at C.G, which increases the difference between strain diagrams of N.F equals zero and N.F acting at S.C. This explains the decrease in cracked axial stiffness in the case of N.F acting at S.C compared to the N.F acting at C.G case. Also, a similar behaviour is noted in Figure 10b for the tension force case, as in case of N.F acting at S.C, the strain diagram is rotated anticlockwise in the same direction compared to the N.F acting at C.G which is rotated also anticolckwise. This behaviour increases the denominator of the cracked axial stiffness and also decreases the cracked axial stiffness.

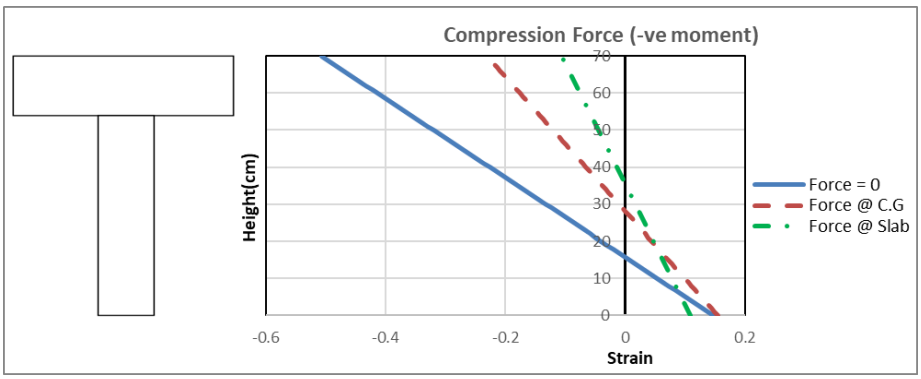

a. Compression force

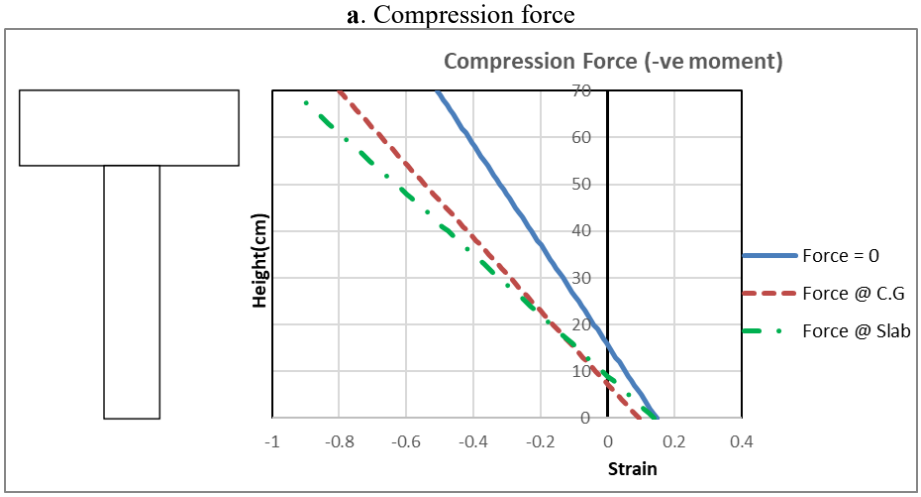

b. Tension force

Figure 10. : Strain distribution along T-Beam depth for -ve moment case using Method 1B&2B.

V. Parametric Study

The effect of different parameters is studied here including the change in beam depth, slab thickness and width and percentage of steel reinforcement. The parametric study performed here is based on approaches 1A and 1B regarding the axial forces acting at the C.G as it is the most common case, where forces are transmitted between columns and beams. A summary of the investigated parameters used in the analysis is provided in Table 2.The effect of each parameter is studied individually while all other parameters are fixed. The base model used here is a beam with dimensions 25 cm x 70 cm and slab width and thickness are 115 cm and 15 cm respectively with a total percentage of steel reinforcement equal to 0.5% which is above the minimum reinforcement which is 0.25% for this beam section.

Table 2. Summary of the investigated parameters.

Parameter	Variation	Unit
Beam depth	70-80-90	cm
Slab thickness	12-15-18	cm
Slab width	25-70-115	cm
Reinforcement ratio	0.5-0.67-0.8	%

Effect of beam depth

The effect of increasing beam depth on SRFs for the +ve moment case is shown in figure 11.a. For the same value of reinforcement percentage, the SRFs for beams with different beam depths are similar with a small difference observed in the high compression and tension force values. For high levels of compression forces, beams with larger depths have higher SRFs. This is because the compression force causes closure of T-beam cracks, and those beams have higher uncracked axial stiffness which reduces cracks in this case due to their bigger dimensions which leads to higher SRFs. As for high levels of tension forces, beams with larger depths have smaller SRFs. The reason for this in the +ve moment case is that the flange is under compression. As the beam depth increases, the ratio of flange area to the total T-beam section area decreases. The compressed flange area is relatively decreased in this case which results in lower values for SRFs.

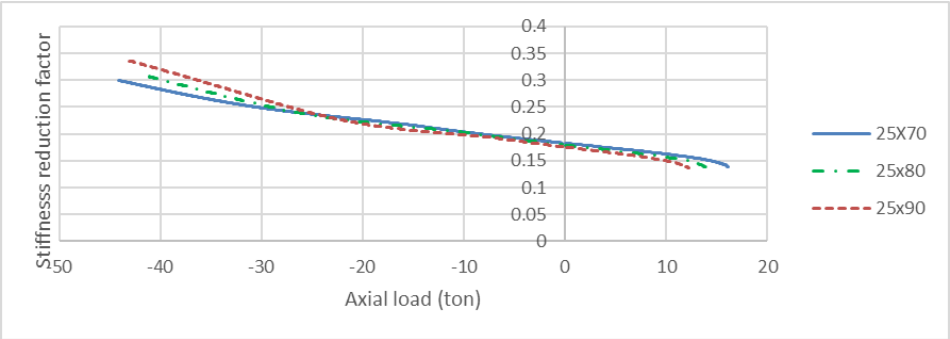

a. +ve moment

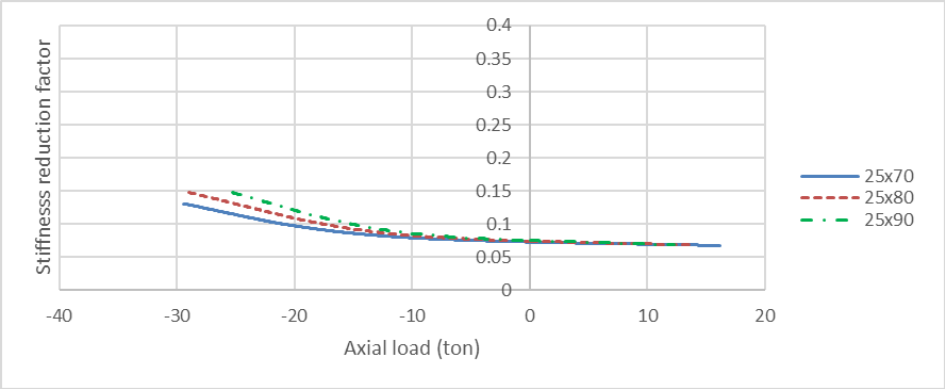

b. -ve moment

Figure 11. : Variation of stiffness reduction factor with axial load for sections with different beam depths.

Figure 11.b shows the effect of beam depth on SRFs in the -ve moment case. In this case, SRFs show a similar behaviour to the +ve moment case with a little difference noted in the tension force zone. Beams with different depths have almost the same modifier values. In -ve moment case, the flange is in tension, and at high levels of tension forces a large portion of the section is cracked and only a small area in the web is still uncracked. When comparing this area to the total section area for the different three depths depths, it is almost the same which results in almost the same SRFs.

Effect of slab thickness

The effect of increasing slab thickness on reduction factors is shown in Figure.12a &12b. For both cases of +ve & -ve moment, reduction factors for sections with larger slab thickness are higher than those with smaller slab thickness. It can be explained by the increase in flange area for sections with larger thickness. As the flange contributes highly to the reduction factors, this increase in flange area results in higher SRFs.

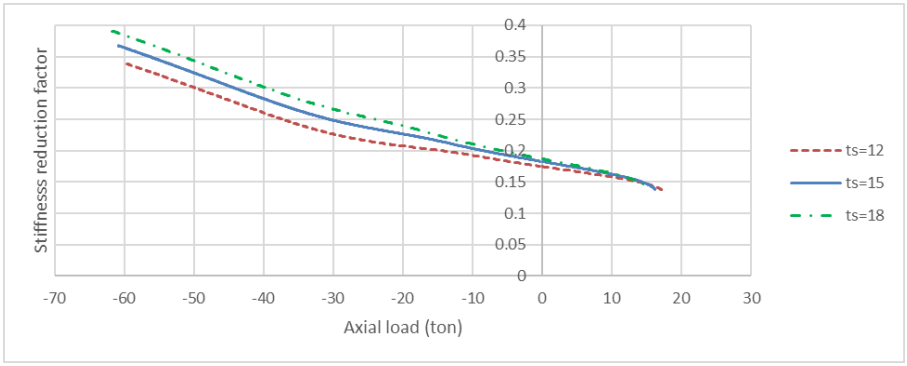

a. +ve moment

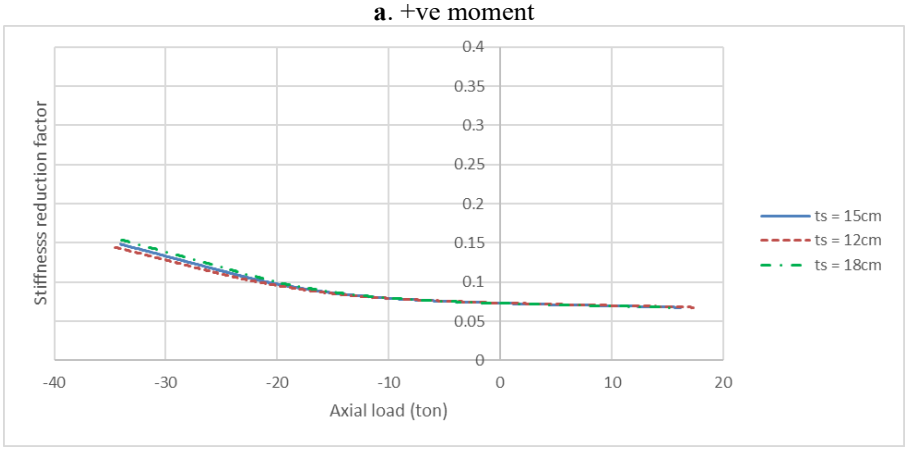

b. -ve moment

Figure 12.:Variation of stiffness reduction factor with axial load with the change is slab thicknesses

Effect of slab width

Figure.13.a, shows the effect of increasing slab width on the reduction factor in +ve moment case. Slab width equal to 25 cm represents the R-section case, in which the width of the beam and slab is the same. As shown in the figure, increasing slab width results in higher values for reduction factors as the compressed flange results in higher reduction factors as the flange has a higher effect on the T-beam stiffness as mentioned before.

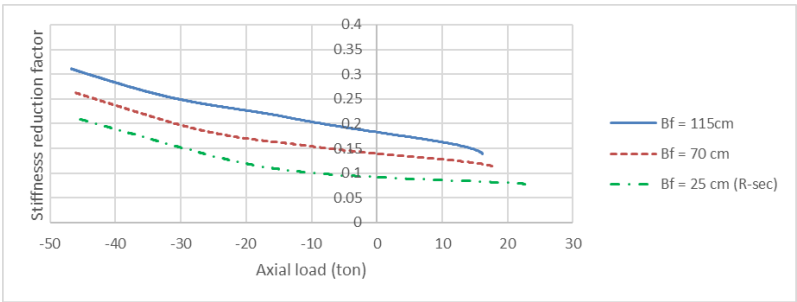

a. +ve moment

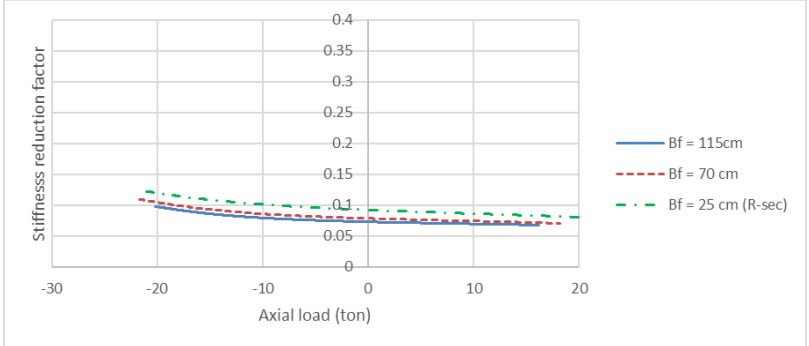

b. -ve moment

Figure 13. : Variation of stiffness reduction factor with axial load with the change in slab width

On the other hand, Figure.13.b shows the effect of increasing slab width on the reduction factor in -ve moment case. In this case, increasing slab width results in lower values for reduction factors, as the flange in tension which results a decrease in the T-beam SRFs .

Effect of Steel reinforcement

The effect of the amount of steel reinforcement in the beam section on the stiffness reduction factors is shown in Figure. 14a and 14b. As shown in the figure, for both cases of +ve and -ve moment, increasing the amount of steel reinforcement produces higher SRFs. This increase is almost a vertical shift in the reduction factors curve for both the compression and tension force cases. As the amount of steel increases, the cracks in T-beam section decrease.

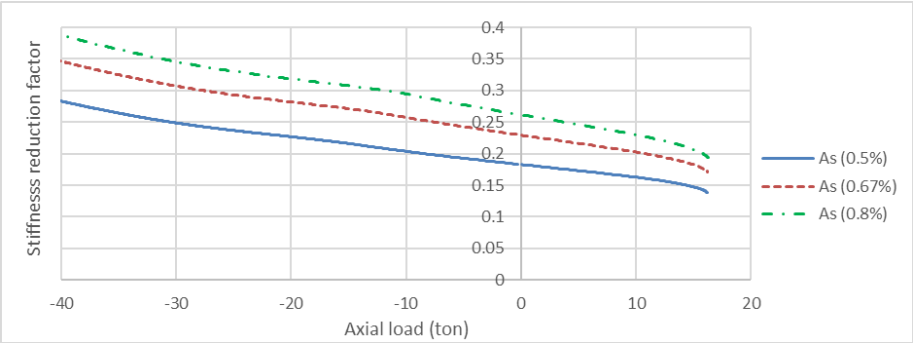

a. +ve moment

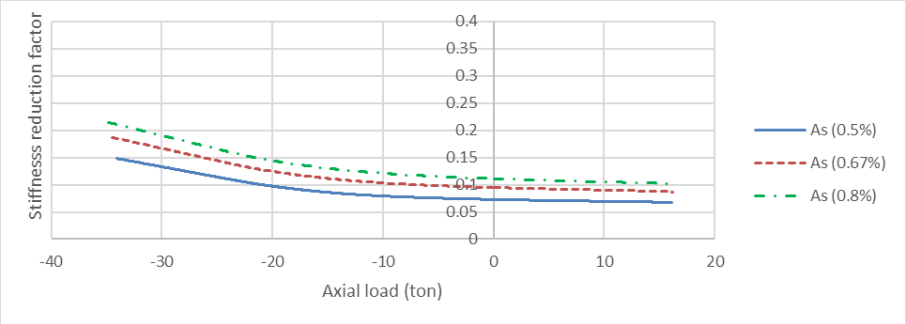

b. -ve moment

Figure 14. : Variation of stiffness reduction factor with the change in steel reinforcement percentage.

The significant increase in reduction factors in this case refer to that the use of fixed values for reduction factors in the thermal analysis of buildings is not appropriate. The reduction factors values used in the analysis should be related to the percentage of steel reinforcement in the beam section.

VI. Summary And Conclusions

In this research, the problem of temperature effect on reinforced concrete structures was studied with a focus on assumptions regarding axial stiffness reduction factors which shall be used in the finite element modeling for these buildings under thermal loading. A new analytical algorithm is developed to consider for the effect of bending cracks on the beams' and slabs' axial stiffness. A software package is developed to calculate T-beam stiffness reduction factors based on charts drawn between the applied axial force and the resulting displacements. Two approaches were used to study the effect of the point of application of the axial force along the T-beam corss-section on the stiffness reduction factors to consider for two cases of load application, one at the T-beam centroid and the other at the slab center. Moreover, a parameteric study was performed to study the effect of section dimensions and beam steel reinforcement on SRFs values. Finally, the conclusions can be summarized as follows:

1. Cracked axial stiffness of T beams is less than their gross axial stiffness under the effect of bending moments resulting from vertical loads.
2. The developed algorithm is able to track the effect of cracking in T-beams and can predict their cracked axial stiffness under any level of normal forces leading to determining the axial stiffness reduction factors.
3. T-beam stiffness reduction factors incresae when the compressive force increases due to the closure of cracks which results in higher stiffness values.

4. T-beam stiffness reduction factor decreases when tensile forces increase due to producing extra cracks which results in smaller stiffness values.
5. Stiffness reduction factors for +ve moment case are higher than those of -ve moment case since the large area of flange contributes highly to the axial stiffness value; hence, in +ve moment case, the flange is under compression resulting in higher uncracked area of the section with higher SRFs.
6. Stiffness reduction factor in case of axial force acting at slab center is increased in +ve moment case and is decreased for -ve moment case compared to the case of axial force acting at the section centroid.
7. Steel reinforcement percentage is the factor with the highest impact on stiffness reduction factors, causing an increase in SRFs values by increasing steel reinforcement percentage.
8. Higher slab thicknesses contribute more in section area under compression resulting in increasing stiffness reduction factors.
9. Increasing slab width results in increasing stiffness reduction factor for +ve moment case and decreasing these factors in -ve moment case.
10. In general, the obtained stiffness reduction factors varied between 0.2-0.5 in case of +ve moment and between 0.05-0.15 in case of -ve moment which is far less than the actual uncracked axial stiffness

In most cases, the RF values are less than 0.5, which indicates that the 50% factor commonly used by designers is rather conservative. Based on the above results, some recommendations can be deduced as follows:

11. When an accurate finite element model is prepared to investigate the effect of temperature, it is important to define different sections under positive and negative moments by varying section stiffness modification coefficients, in order to simulate the cracking effect on the actual sections' behaviour.
12. In finite element analysis, sections should be defined with different values for stiffness reduction factors with the change in the percentage of steel reinforcement in beam sections.
13. The determination of more accurate values for stiffness reduction factors will help in the actual simulation of the temperature effect on RC buildings which consequently results in more realistic and lower values for the straining actions on the supporting columns.

References

[1]. ACI Committee 349.1R-4, Reinforced Concrete Design For Thermal Effects On Nuclear Power Plant Structures.
[2]. ACI Committee 224.2R-92, Cracking Of Concrete Members In Direct Tension, ACI Structural Journal, 1992, Pp. 6:7.
[3]. ECP 203 (2020), Design & Construction Of Concrete Structures, Pp. 6-22.
[4]. Heba A. Goda, Hisham A. El-Arabaty, Nasr E. Nasr , Bahaa Sharaf Turk, Assessment Of Flat Slab Axial Stiffness In Thermal Analysis, Al-Azhar University Civil Engineering Research Magazine (CERM) Vol. (44) No. (1) January 2022.
[5]. Mohamed A. Abdul Rahim, Hisham A. El-Arabaty, Gamal H. Mahmoud, Nasr E. Nasr, Finite Element Modelling Of Structures Subjected To Thermal Loading, IOSR-JMCE Journal, Vol. 15, No. 6, 2018, Pp. 31-43.
[6]. Mohamed A. Abdul Rahim, Hisham A. El-Arabaty, Gamal H. Mahmoud, Nasr E. Nasr, Interactive Implementation Of Axial Stiffness Reduction Factors In Thermal Analysis Of Multistory Buildings IOSR,Journal Of Mechanical And Civil Engineering (IOSR-JMCE).
[7]. M. Mehdi Mirzazadeh, Mark F. Green, Non-Linear Finite Element Analysis Of Reinforced Concrete Beams With Temperature Differentials, ELSEVIER Journal, 2017, Volume 152, Pages 920-933.
[8]. Salah E. El-Metwally, Essam H. El-Tayeb, Ahmed M. Yousef, Analysis Of RC Flat Slab System For Thermal Loads, IJEIT Journal, 2015, Volume 4, Issue 12.
[9]. Salah E. El-Metwally, Mohamed E. El-Zoughiby, Reda M. Elgarayhi, Shrinkage And Thermal Effects In R/C Flat Plate And Raft Foundation, Engineering Research Journal, 2019